Acta Biochim Biophys Sin 2026, Vol.(1): fpage–lpage
https://cstr.cn/32197.14.abbs.2026101
https://doi.org/10.3724/abbs.2026101
Original Article

Original Article

ACBD3 promotes the antiviral innate immune response against vesicular stomatitis virus infection by stabilizing MAVS through TRIM21

Peili Hou†, Yingying Li†, Zhangping Yu†, Xingyu Li†, Hongbin He*, and Hongmei Wang*

Ruminant Diseases Research Center, College of Life Sciences, Shandong Normal University, Jinan 250358, China
†These authors contributed equally to this work.
*Correspondence address. E-mail: hongbinhe@sdnu.edu.cn (H.H.); hongmeiwang@sdnu.edu.cn (H.W.)

Received 22 July 2025 Accepted 18 March 2026 Published 7 August 2026

Abstract

Acyl-CoA binding domain containing protein 3 (ACBD3) is a Golgi protein implicated in multiple cellular processes. However, its function in negative-strand RNA virus infection and innate immune responses remains poorly understood. Here, we identify ACBD3 as a novel positive regulator of host defense that potently inhibits vesicular stomatitis virus (VSV) replication in HeLa cells with ACBD3 overexpression or knockdown. Mechanistically, our investigation unveils a previously unknown ACBD3-TRIM21-MAVS axis. Co-immunoprecipitation combined with mass spectrometry analysis reveals that ACBD3 interacts with the E3 ubiquitin ligase TRIM21, and this interaction is crucial for stabilizing the mitochondrial antiviral-signaling protein (MAVS). During VSV infection, ACBD3 enhances TRIM21 protein levels, thereby promoting MAVS accumulation and facilitating the activation of type I interferon signaling. Collectively, our findings elucidate a novel mechanism by which ACBD3 sustains innate immunity via TRIM21 to restrict VSV replication, providing a potential therapeutic target and strategy for combating negative-strand RNA viruses.

Key words acyl-CoA binding domain containing protein 3, vesicular stomatitis virus, mitochondrial antiviral signaling protein, type I interferon, TRIM21

Introduction

Vesicular stomatitis, caused by vesicular stomatitis virus (VSV), is a zoonotic disease affecting livestock such as pigs, horses, and cattle, as well as humans [1,2]. Given the high transmissibility, propensity for widespread outbreaks, and specificity associated with antibody-mediated protection, no effective vaccine against VSV is currently available. As a prototypical member of the negative-strand RNA virus, VSV is not only an important veterinary pathogen but also a classic model for studying the cellular innate immune response [3–5]. Understanding how VSV regulates cellular innate immune signaling pathways is crucial for comprehending host antiviral defense mechanisms.

Cellular innate immune responses serve as the first line of host defense against viruses and other pathogens [6]. During viral invasion, cytokines such as interferon and interferon-stimulating genes (ISGs) are induced, enhancing the antiviral immune response [7]. A central pathway in this response is the RIG-I-MAVS signaling axis, which plays a pivotal role in initiating type I interferon (IFN-I) production [8,9]. Regulation of the MAVS signaling pathway can occur through various mechanisms, including the disruption of interactions between MAVS and downstream signaling molecules or inducing degradation of MAVS mediated by host factors and viral proteins [10]. For instance, the E3 ubiquitin ligase RING finger protein 114 can negatively regulate MAVS to suppress IFN-I production [11]. Conversely, host proteins such as REC8 can stabilize MAVS and promote antiviral signaling [12]. Additionally, TRAF3-interacting protein 3 suppresses VSV replication through inhibiting the RIG-I-MAVS-TBK1 signaling axis [13]. Despite these advances, the complete regulatory network governing MAVS stability and function remains incompletely elucidated.

Acyl-CoA binding domain containing protein 3 (ACBD3), which contains an acyl-coenzyme A binding domain, is a multifunctional protein primarily involved in maintaining the structure of the Golgi apparatus and regulating intracellular transport between the endoplasmic reticulum (ER) and the Golgi apparatus [14]. Structurally, the GOLD domain of ACBD3 serves as the target for

© The Author(s) 2026. This is an open access article distributed under the terms of the Creative Commons Attribution-NonCommercial-NoDerivs License (https://creativecommons.org/licenses/by-nc-nd/4.0/).

interactions with viral 3A proteins of Aichi virus (AiV) and enterovirus A71 (EV71) [15,16]. Notably, ACBD3 has been implicated in promoting the replication of several positive-strand RNA viruses through interaction with viral proteins [16]. However, its role during infection with negative-strand RNA viruses such as VSV remains unknown. Notably, our preliminary RNA-seq data revealed a significant upregulation of *ACBD3* expression in VSV-infected cells, leading us to hypothesize that ACBD3 might play a previously unrecognized role in the process of VSV infection.

In this study, we identify ACBD3 as an antiviral host factor that inhibits VSV replication. To elucidate the mechanism, we demonstrate that ACBD3 interacts with the E3 ubiquitin ligase TRIM21, which is critical for stabilizing the innate immune adaptor MAVS, thereby potentiating the type I interferon response. Collectively, our findings define the ACBD3-TRIM21-MAVS axis as a key regulator of antiviral immunity, highlighting a new path for therapeutic development.

Materials and Methods

Cell lines and viruses

The HeLa (TCHu187), Vero (GNO10), and HEK293T (GDC0067) cell lines were obtained from the Typical Culture Preservation Committee Cell Bank of the Chinese Academy of Sciences (Shanghai, China). Cells were maintained in Dulbecco's modified Eagle medium (DMEM, 11995065; Gibco, Grand Island, USA) supplemented with 10% fetal bovine serum (FBS, A5256701; Gibco), 100 U/mL penicillin G / 100 μg/mL streptomycin sulfate (15070063; Gibco), and incubated at 37°C in 5% CO_2. The attenuated VSV strain and VSV-eGFP strain were established as previously described [17]. Briefly, viruses were amplified in Vero cells, and quantified via plaque assay and stored at −80°C for subsequent infection experiments.

Antibodies and reagents

Antibodies against RIG-I (D14G6, 3743), MDA-5 (D74E4, 5321), TBK1 (D1B4, 3504), phospho-TBK1 (Ser172, D52C2, 5483), DYKDDDDK/FLAG Tag (D6W5B, 14793), and HA-Tag (C29F4, 3724) were obtained from Cell Signaling Technology (Danvers, USA). Antibodies against VSV-G (AB0053), GFP (AB0045), β-tubulin (AB0039), IRF3 (CY5779), phospho-IRF3 (S386, CY6575), GAPDH (AB0037), and β-actin (AB0061) were acquired from Abways Technologyn (Shanghai, China). Anti-MAVS antibody (sc-166583) was sourced from Santa Cruz Biotechnology (Dallas, USA). Anti-ACBD3 (14096-1-AP) and anti-TRIM21 (A02079-2) polyclonal antibodies were purchased from Proteintech Group (Wuhan, China) and Boster Biological Technology (Wuhan, China). Chemical reagents, including chloroquine (HY-17589A), MG132 (HY-13259), Z-VAD (HY-164388), and bafilomycin A1 (HY-100558), were supplied by MedChemExpress (Shanghai, China). Protein markers (WJ101) for western blotting were obtained from Epizyme Biotech (Shanghai, China).

Plasmids and siRNAs

The coding sequences (CDS) of human MAVS, TRIM21, and ACBD3 were amplified based on the following reference sequences: *MAVS* mRNA (GenBank No. NM_020744.5), *TRIM21* mRNA (GenBank No. NM_003141.4), and *ACBD3* mRNA (GenBank No. NM_022735.4). These CDS regions were subsequently cloned and inserted into plasmid vectors to generate overexpression constructs containing the indicated tags, as well as a series of ACBD3 domain mutants. pLV2-CMV-Mito-mCherry-Puro was purchased from MiaoLing Bio (Wuhan, China). All primer names and sequences used for plasmid construction are provided in Supplementary Table S1. For gene silencing experiments, siRNA synthesized by Sangon Biotech (Shanghai, China) targeting *ACBD3* (5′-GGAUGCA GAUUCCGUGAUU-3′) and a non-targeting control siRNA (5′-GCUGUCGUCCUCAAUUCUATT-3′) were employed.

Quantitative real-time PCR and western blotting

Polyinosinic-polycytidylic acid, poly(I:C), a synthetic analog of double-stranded RNA, was transfected into cells with ACBD3 overexpression and knockdown. Gene expression levels of *VSV-P*, *IFNB*, *ISG56*, *CCL5*, and *TRIM21* were analyzed by quantitative real-time PCR (qPCR). Total RNA was extracted from cultured cells and reverse-transcribed into cDNA using the Accurate Reverse Transcription Kit (AG11706; Accurate Biology, Changsha, China). qPCR was performed with AceQ qPCR SYBR Green Master Mix (Q111-02; Vazyme, Nanjing, China) on a Roche Real-Time PCR System (05015278001; Roche, Basel, Switzerland) following the manufacturer's protocol. Briefly, the reaction mixture was prepared and subjected to pre-denaturation, cyclic amplification and melting curve analysis. Relative gene expression levels were calculated via the $2^{-\Delta\Delta Ct}$ method with *β-actin* used as the internal reference gene. All sequences of primers used for target and reference gene amplification are provided in Supplementary Table S2.

For western blotting, cells were harvested and lysed in RIPA buffer (Beyotime, Shanghai, China) containing a protease inhibitor cocktail (HY-K0010; MedChemExpress). Protein lysates were resolved by 12.5% SDS-PAGE and transferred to PVDF membranes. After blocking with 5% skim milk, the membranes were incubated with the indicated primary antibodies, followed by HRP-conjugated secondary antibodies (111035003; Jackson ImmunoResearch, West Grove, USA). Protein signals were detected using an enhanced chemiluminescence (ECL) kit (ED0015-C; Sparkjade Biotechnology, Jinan, China).

Immunoprecipitation and co-immunoprecipitation

For immunoprecipitation assays, HEK293T cells were transfected with either pLVX-Flag-ACBD3 or the empty pLVX vector (Clontech, Mountain View, USA), followed by infection with VSV at an MOI of 0.1. After 24 h, the cells were harvested and lysed in non-denaturing lysis buffer. The lysates were incubated with anti-Flag magnetic beads (AP62L172; MCL, Shanghai, China) to enrich ACBD3-interacting proteins. The immunoprecipitated complexes were separated by 12.5% SDS-PAGE, and the gel strips were subjected to mass spectrometry analysis by JINGJIE Biotech (Hangzhou, China) to identify potential binding partners of ACBD3. For co-immunoprecipitation (Co-IP) analysis, HEK293T cells were co-transfected with GFP-ACBD3, Flag-TRIM21, or the HA-MAVS plasmid, and cells were harvested after 36 h. The cells were lysed for 1 h on ice in a native lysis buffer (R0030; Solarbio, Beijing, China) supplemented with 1 mM protlytic protease inhibitor cocktail (P002; New Cell & MolecularBiotech, Suzhou, China). Cell lysates were then centrifuged, and the supernatant was incubated with anti-GFP or anti-Flag magnetic beads (Smart-Life sciences, Changzhou, China) for 2 h at 4°C. After washing with cold lysis buffer, the proteins were detected by western blot analysis.

Luciferase reporter assay

HEK293T cells were seeded in 96-well plates and were then co-transfected with 160 ng IFN-β promoter-driven firefly luciferase reporter plasmid ($pGL_{3.0}$-IFN-β) (MiaoLing Bio), 20 ng pRL-TK plasmid expressing Renilla luciferase (as an internal control) (MiaoLing Bio), 200 ng vector or Flag-ACBD3, and 100 ng innate immune node molecule plasmid (RIG-I-N, MDA5, MAVS, TBK1, IKKε, or IRF3-5D, respectively). After 24 h of transfection, the dual-specific luciferase kit (DL10101; Vazyme, Nanjing, China) was used to evaluate the ratio of Firefly luciferase activity to Renilla luciferase activity on a SpectraMax M5 microplate reader (Molecular Devices Instruments Inc., Sunnyvale, USA), and the relative luciferase activity was normalized using data from the control group.

Confocal fluorescence microscopy

The subcellular localization and potential co-localization of ACBD3 and MAVS were examined by confocal microscopy. HeLa cells were transfected with Flag-tagged ACBD3 and HA-tagged MAVS plasmids using Attractene transfection reagent (310007; Qiagen, Venlo, Netherlands). After 24 h, the cells were fixed with 4% paraformaldehyde (P1110; Solarbio) for 10 min and permeabilized with 0.1% Triton X-100 (9410-OP; Millipore, Burlington, USA) for 10 min at room temperature. Following three PBS washes, the samples were blocked with 5% BSA (A8806; Sigma-Aldrich, St Louis, USA) for 1 h and then incubated sequentially with primary antibodies and fluorophore-conjugated secondary antibodies. The nuclei were stained with DAPI (C0065; Solarbio). Images were captured using the Leica confocal microscope (Leica DMIRBE inverted microscope; Leica, Solms, Germany).

Generation of *TRIM21*-knockout (KO) cell lines through the CRISPR–Cas9 system

TRIM21-knockout HeLa cell lines were constructed using the lenti-CRISPR/Cas9-V2 system. The guide RNA (gRNA) sequences targeting *TRIM21*, listed in Supplementary Table S1, were designed via the online tool CRISPR Direct (http://crispr.dbcls.jp/). Single-cell clones of *TRIM21*-knockout cells were selected with puromycin (P8230; Solarbio), and their knockout efficiency was subsequently confirmed by western blot analysis.

Viral infection and plaque assays

Cells were infected with VSV for the indicated durations. Viral titers in cell supernatants were determined by plaque assays on Vero cells. Serially diluted supernatants were added to confluent cells in 24-well plates. After 1 h of incubation, the medium was replaced with 1% methylcellulose (M7027, Sigma-Aldrich) overlay. At 3 d post-infection, the overlay was discarded. Cells were fixed with 4% formaldehyde (F8775; Sigma-Aldrich) for 1 h and stained with 1% crystal violet (C3886; Sigma-Aldrich) in 20% methanol. Plaques were counted by Image J, averaged and multiplied by the dilution factor to determine viral titer as PFU/mL.

Statistical analysis

All statistical analyses were performed using GraphPad Prism 8.0. Comparisons between two groups were conducted using Student's *t* test, while multiple comparisons among three or more groups were analyzed by one-way or two-way ANOVA, as appropriate. The results are presented as the mean ± standard deviation (SD) from at least three independent experiments. *P* values less than 0.05 considered statistically significant.

Results

ACBD3 inhibits VSV replication

While ACBD3 has been established to influence positive-strand RNA viruses, its role in the replication of negative-strand RNA viruses remains unexplored. To investigate the role of ACBD3 in the replication of VSV, the effects of the overexpression or knockdown of ACBD3 in HeLa cells on the transcriptional levels of the *VSV-P* gene and the protein levels of VSV-G were examined. The results showed that overexpression of ACBD3 led to significant suppression of *VSV-P* mRNA levels (Figure 1A) and VSV-G protein synthesis (Figure 1B) compared with controls. Conversely, when *ACBD3* was knocked down using siACBD3 prior to VSV infection, *VSV-P* mRNA (Figure 1C) and VSV-G protein levels (Figure 1D) were markedly enhanced relative to control siRNA-treated cells. Furthermore, HeLa cells with either ACBD3 overexpression or knockdown were infected with VSV-eGFP, and the fluorescence intensity of GFP was evaluated by fluorescence microscopy. Consistently, compared to the control groups, overexpression of ACBD3 significantly reduced GFP fluorescence intensity and inhibited replication of VSV-eGFP. Conversely, silencing of *ACBD3* had the opposite effect (Figure 1E and Supplementary Figure S1). Collectively, these results demonstrate that ACBD3 inhibits VSV replication.

ACBD3 activates the type I interferon signaling pathway

The type I interferon signaling pathway, especially the activation of IFN-β, further induces the expression of downstream interferon-stimulating genes (ISGs), thus exerting antiviral functions. To determine whether ACBD3 regulates the type I interferon signaling pathway, the expression levels of type I interferon pathway-related molecules in VSV-infected HeLa cells with ACBD3 overexpression and knockdown were detected. As shown in Figure 2A, ACBD3 overexpression enhanced the transcription of *IFNB* and *ISGs* (including *CCL5* and *ISG56*) in response to VSV infection. Consistent with this, dual luciferase reporter assays demonstrated that ACBD3 significantly potentiated *IFN-β* promoter activity under the same conditions (Figure 2B). At the protein level, ACBD3 overexpression also promoted VSV-induced phosphorylation of TBK1 and IRF3 (Figure 2C). Conversely, *ACBD3* knockdown had the opposite effect (Figure 2D,E). Furthermore, poly(I:C), a synthetic analog of double-stranded RNA, was transfected into cells to investigate the broad-spectrum antiviral role of ACBD3. qPCR analysis revealed that ACBD3 overexpression enhanced the transcription of *IFNB*, *CCL5*, and *ISG56* following poly(I:C) stimulation (Figure 3A). Conversely, *ACBD3* knockdown produced the opposite effects (Figure 3B). At the protein level, ACBD3 overexpression enhanced the phosphorylation and activation of both TBK1 and IRF3 in response to poly(I:C) (Figure 3C). In contrast, *ACBD3* knockdown inhibited these signaling molecules (Figure 3D). These findings suggest that ACBD3 can activate both VSV and the poly(I:C)-induced type I interferon signaling pathway.

ACBD3 promotes the antiviral immune response by targeting MAVS

As previously established, VSV infection activates the RLR signaling pathway. To investigate the specific regulatory mechanism, ACBD3 was co-transfected with different RLR signaling pathway-related genes in HEK293T cells, and the activity of the *IFN-β* promoter was

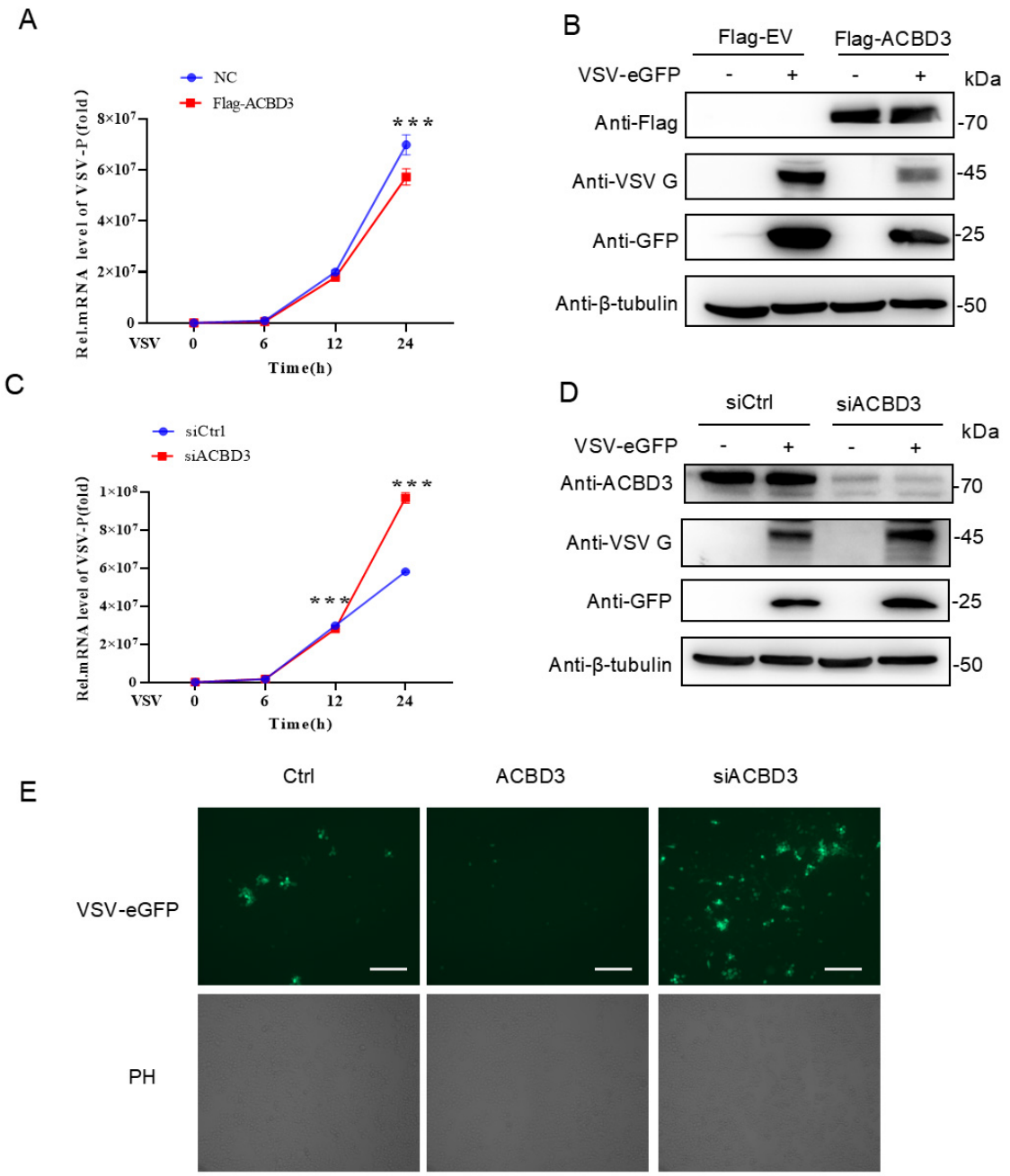


Figure 1. ACBD3 inhibits VSV replication in HeLa cells (A) qPCR analysis of VSV-*P* gene mRNA transcription in Flag-ACBD3-overexpressing HeLa cells infected with VSV (MOI = 0.1) for 0 h, 6 h, 12 h, and 24 h. (B) Western blot analysis of VSV-G protein levels and VSV-tagged GFP levels in Flag-ACBD3-overexpressing HeLa cells infected with VSV-eGFP (MOI = 0.1) for 24 h. (C) *VSV-P* mRNA transcription in HeLa cells after *ACBD3* knockdown using siRNA and infected with VSV (MOI = 0.1) for 0 h, 6 h, 12 h, and 24 h. (D) VSV-G protein levels and VSV-tagged GFP levels in HeLa cells after *ACBD3* knockdown and infected with VSV-eGFP (MOI = 0.1) for 24 h. (E) Phase-contrast (PH) and fluorescence microscopy analysis of ACBD3-overexpressing and *ACBD3*-silenced cells infected with VSV-eGFP (MOI = 0.1) for 24 h. Scale bar: 100 μm. All statistical analyses were performed using GraphPad Prism 8.0. Comparisons between two groups were conducted using two way-ANOVA. The results are presented as the mean ± standard deviation (SD) from at least three independent experiments (***$P < 0.001$).

analyzed. ACBD3 enhanced promoter activation triggered by RIG-I-N (N-terminal CARDs), MDA5, and MAVS but not TBK1, IKKε and IRF3-5D (a constitutively active form of IRF3), suggesting that it might target MAVS to potentiate type I interferon responses (Figure 4A). We next performed western blot analysis in *ACBD3*-silenced HeLa cells to assess the RLR signaling pathway upon VSV infection. While the MAVS protein level was significantly decreased at 6 and 12 h post-infection, *ACBD3* knockdown did not notably affect the expression of RIG-I, MDA5, TBK1, or IRF3 (Figure 4B). Furthermore, GFP-ACBD3 and HA-MAVS were co-transfected into HEK293T cells, and their interaction was validated using co-immunoprecipitation (Figure 4C). Furthermore, confocal microscopy revealed that VSV infection induced the translocation of ACBD3 to mitochondria and facilitated the co-localization of ACBD3

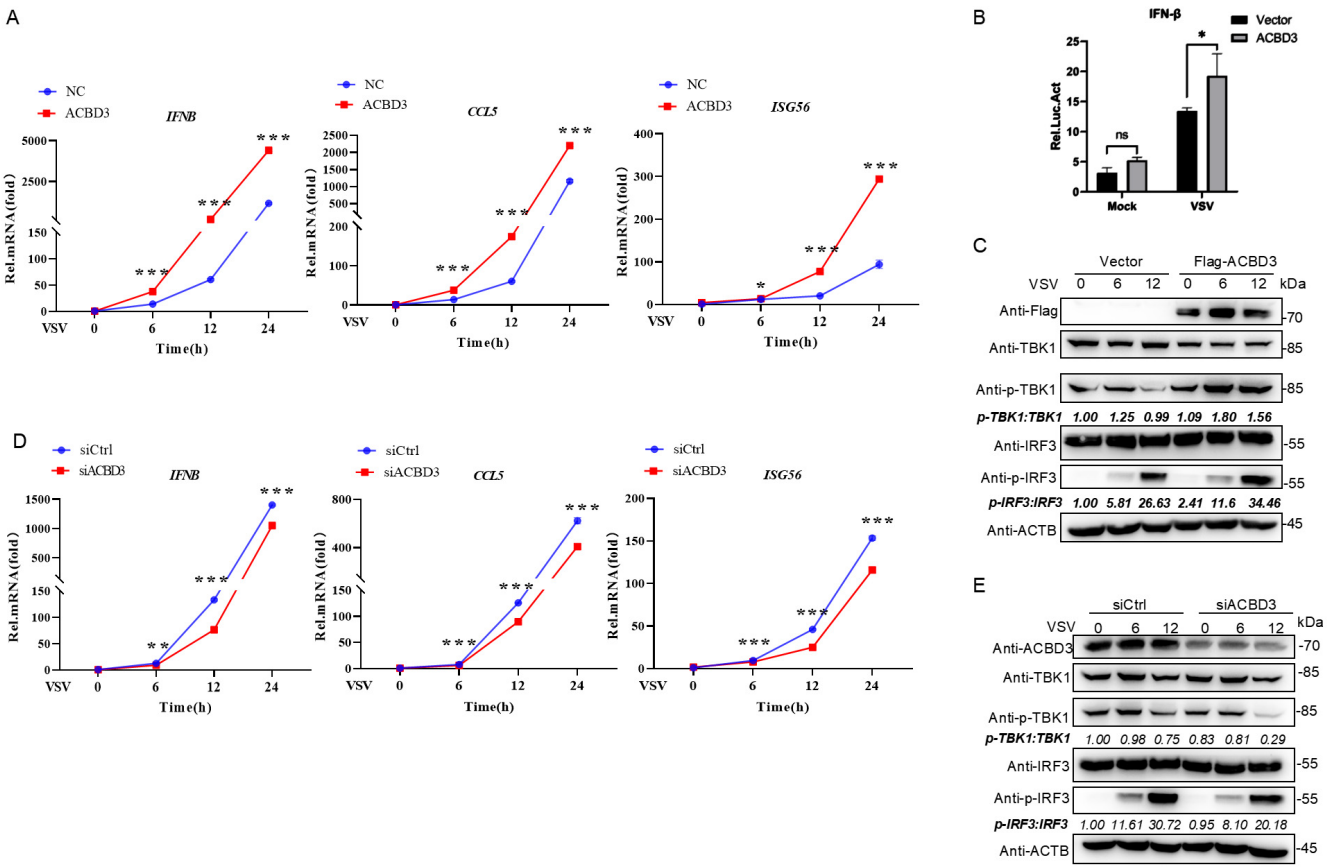


Figure 2. ACBD3 activates the VSV-triggered type I interferon signaling pathway in HeLa cells (A) qPCR analysis of *IFNB*, *CCL5*, and *ISG56* gene transcription in ACBD3-overexpressing cells infected with VSV (MOI = 0.1) for 0 h, 6 h, 12 h, and 24 h. (B) Luciferase reporter assays of *IFN-β* promoter activity in ACBD3-overexpressing cells infected with VSV (MOI = 0.1). (C) Western blot analysis of TBK1 and IRF3 phosphorylation in ACBD3-overexpressing cells infected with VSV (MOI = 0.1) for 0 h, 6 h, and 12 h. (D) qPCR analysis of *IFNB*, *CCL5*, and *ISG56* gene transcription in *ACBD3*-silenced cells infected with VSV (MOI = 0.1) for 0 h, 6 h, 12 h, and 24 h. (E) Western blot analysis of TBK1 and IRF3 phosphorylation in *ACBD3*-silenced cells infected with VSV (MOI = 0.1) for 0 h, 6 h, and 12 h. All statistical analyses were performed using GraphPad Prism 8.0. Comparisons between two groups were conducted using two way-ANOVA. The mean and SD from least three independent experiments are shown (*ns* $P > 0.05$, *$P < 0.05$, **$P < 0.01$, and ***$P < 0.001$).

and MAVS (Figure 4D, Supplementary Figure S2). To further delineate the specific domain of ACBD3 involved in this interaction, truncated mutants of ACBD3 were generated (Figure 4E). Co-IP assays in HEK293T cells expressing HA-MAVS together with full-length or truncated ACBD3 showed that both the full-length protein and the 360–523 fragment interacted with MAVS, indicating that the GOLD domain of ACBD3 mediates this binding (Figure 4F). Taken together, these results demonstrate that ACBD3 promotes an antiviral innate immune response by targeting MAVS.

ACBD3 promotes the interaction between TRIM21 and MAVS

To further explore how ACBD3 regulates MAVS during VSV infection, *MAVS* mRNA levels were determined. ACBD3 did not regulate MAVS expression at the transcriptional level upon VSV infection (Supplementary Figure S3). To determine ACBD3's role in prolonging the MAVS half-life, cycloheximide chase was added to control and *ACBD3*-knockdown cells. In control cells, MAVS protein levels remained stable over the 24-h chase period. In contrast, upon *ACBD3* knockdown, MAVS degradation was markedly accelerated. This finding demonstrates that ACBD3 is required to maintain MAVS stability by preventing its degradation (Supplementary Figure S4). Additionally, MAVS protein expression was determined in *ACBD3*-silenced cells treated with the appropriate final concentrations of the caspase inhibitor Z-VAD (10 μM), ubiquitin proteasome inhibitor MG132 (10 μM), autophagolysosomal inhibitors chloroquine (CQ, 40 μM) and bafilomycin A1 (BafA1, 1 μM). As shown in Figure 5A, the decrease in MAVS levels induced by *ACBD3* knockdown was rescued by MG132 but not by CQ, BafA1, or Z-VAD, indicating that ACBD3 protects MAVS from degradation primarily via the ubiquitin-proteasome pathway. In addition, the addition of MG132 during VSV infection did not significantly affect the expression of LC3B (Supplementary Figure S5). Then, potential ACBD3-interacting proteins in the process of VSV infection were identified by mass spectrometry analysis. Following ACBD3 overexpression, 0.1 MOI VSV was used to infect HEK293T cells for 24 h. Anti-Flag magnetic agarose beads were utilized to immunoprecipitate ACBD3-associated protein complexes, which were separated by SDS-PAGE and subsequently analyzed by LC-MS/MS to capture potential ACBD3 binding partners (Figure 5B). Among the top 20 candidates listed in Supplementary Table S3, TRIM21 was the only E3 ubiquitin ligase identified as a potential interactor of ACBD3 during VSV infection (Figure 5C). Subsequently, Co-IP assays confirmed that GFP-ACBD3

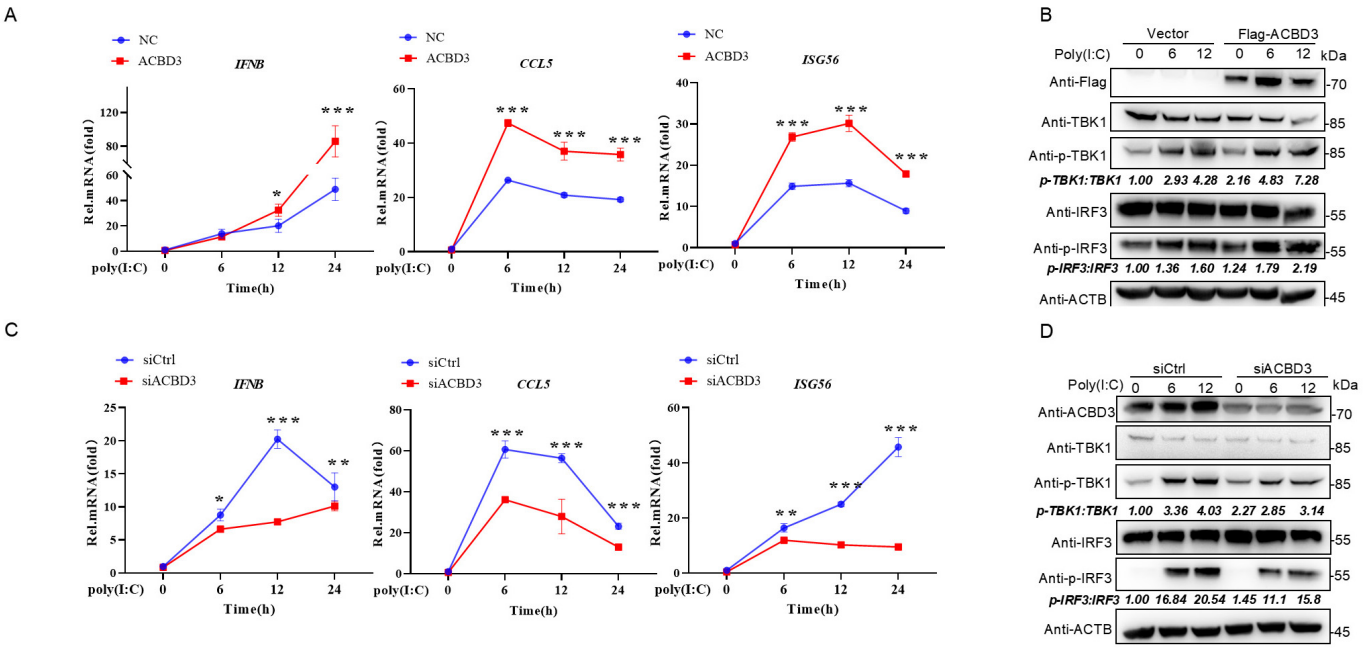


Figure 3. ACBD3 activates the poly(I:C)-triggered type I interferon signaling pathway in HeLa cells (A) qPCR analysis of *IFNB*, *CCL5*, and *ISG56* mRNA in ACBD3-overexpressing cells transfected with poly(I:C) for 0 h, 6 h, 12 h, and 24 h. (B) Western blot analysis of TBK1 and IRF3 phosphorylation in ACBD3-overexpressing cells transfected with poly(I:C) for 0 h, 6 h, and 12 h. (C) qPCR analysis of *IFNB*, *CCL5*, and *ISG56* gene transcription in *ACBD3*-silenced cells transfected with poly(I:C) for 0 h, 6 h, 12 h, and 24 h. (D) Western blot analysis of TBK1 and IRF3 phosphorylation in *ACBD3*-silenced cells transfected with poly(I:C) for 0 h, 6 h, and 12 h. All statistical analyses were performed using GraphPad Prism 8.0. Comparisons between two groups were conducted using two way-ANOVA. The mean and SD from least three independent experiments are shown (*$P < 0.05$, **$P < 0.01$, and ***$P < 0.001$).

specifically precipitated Flag-TRIM21 (Figure 5D). Furthermore, we found that ACBD3 enhanced the interaction between TRIM21 and MAVS (Figure 5E), whereas *ACBD3* knockdown attenuated TRIM21-MAVS complex formation during VSV infection (Figure 5F).

ACBD3 enhances the antiviral effect of TRIM21

Although ACBD3 promotes the interaction between TRIM21 and MAVS, its effect on endogenous TRIM21 expression remains unclear. To explore the function of endogenous TRIM21 affected by ACBD3 during VSV infection, ACBD3 or control plasmids were transfected into HeLa cells. After 24 h, the cells were infected with VSV at an MOI of 0.1. qPCR and western blot analysis revealed that ACBD3 upregulated endogenous TRIM21 expression at both the mRNA (Figure 6A) and protein (Figure 6B) levels during viral infection. TRIM21 stabilizes MAVS expression, which is known to exert broad antiviral activity. ACBD3 altered antiviral action through TRIM21. The results indicated that overexpression of TRIM21 suppressed VSV GFP expression, and this inhibitory effect was further enhanced by co-expression of ACBD3 (Figure 6C). To further examine whether the antiviral function of TRIM21 involves MAVS regulation, we overexpressed TRIM21 in HEK293T cells and infected them with VSV. TRIM21 overexpression reduced MAVS degradation and suppressed VSV GFP expression (Figure 6D). *TRIM21* knockout led to a downregulation of MAVS levels and a corresponding increase in VSV-G expression (Supplementary Figure S6). Furthermore, overexpression of ACBD3 and TRIM21 promoted the ubiquitination of MAVS, demonstrating that MAVS ubiquitination may play an important role in maintaining its stable expression (Supplementary Figure S7). Taken together, these results demonstrate that ACBD3 stabilizes MAVS levels in a TRIM21-dependent manner and that ACBD3 enhances the antiviral effect of TRIM21.

Discussion

While ACBD3 is well known for supporting the replication of various positive-strand RNA viruses [18–21], its role in the process of negative-strand RNA virus infections remains unexplored. Here, we found that ACBD3 acts as a potent antiviral factor against VSV, demonstrating that this host protein can play dual roles in different viral contexts.

The synthesis of interferon and the expression of interferon-stimulated genes are hallmarks of innate immune activation for the host to resist viral infection [22]. This prompted us to ask whether ACBD3 influences antiviral signaling. Our data establish ACBD3 as a positive regulator of the type I interferon pathway. In VSV-infected cells, ACBD3 overexpression enhanced the type I interferon response, while *ACBD3* knockdown diminished the transcription of *IFN-β* and key ISGs. This finding provides a mechanistic explanation for the antiviral effect of ACBD3 against VSV. To our knowledge, this is the first demonstration that ACBD3 can suppress viral replication by activating the innate immune response in the context of a negative-strand RNA virus.

As the central adaptor protein in the RIG-I-MAVS signaling pathway, MAVS is a critical control point for the type I interferon response [23]. Its stability and activity are precisely regulated through various mechanisms, including post-translational modifications and degradation [10], [24]. Precisely how MAVS stability is regulated in different viral contexts remains an active area of investigation. Ubiquitination plays a key role in regulating MAVS stability and activity; for example, E3 ligases such as ankyrin repeat

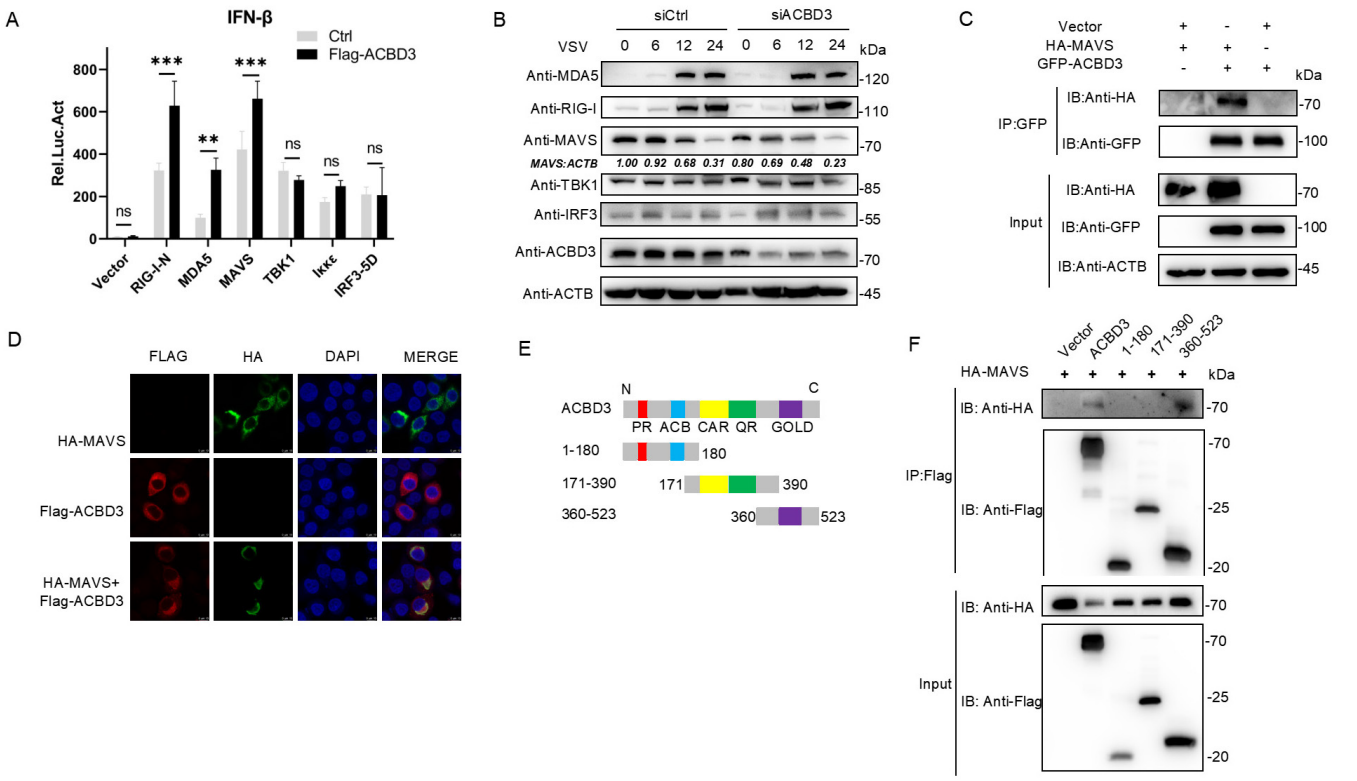


Figure 4. ACBD3 promotes the antiviral natural immune response by targeting MAVS (A) HEK293T cells were transfected with RIG-I-N, MDA5, MAVS, TBK1, IKKε, IRF3-5D, IFN-β luciferase reporter gene, pRL-TK, ACBD3 or empty vector for 24 h. Luciferase activity was measured. All statistical analyses were performed using GraphPad Prism 8.0. Comparisons between two groups were conducted using Student's *t* test. The mean and SD from at least three independent experiments are shown (*ns* $P > 0.05$, $^{**}P \leq 0.01$, and $^{***}P \leq 0.001$). (B) Western blot analysis of RIG-1, MDA5, MAVS, TBK1 and IRF3 in *ACBD3*-silenced cells infected with VSV (MOI = 0.1) for 0 h, 6 h, 12 h, and 24 h. (C) Co-IP analysis of the interaction between ACBD3 and MAVS. (D) The colocalization of ACBD3 and MAVS as revealed by laser confocal approach. Scale bar: 20 μm. (E) Truncated mutants of ACBD3 and (F) their interaction with MAVS as revealed by Co-IP.

and IBR domain containing 1 (ANKIB1) and ankyrin repeat and SOCS box-containing protein 3 (ASB3) promote its degradation, whereas TRIM31 enhances its activation through K63-linked ubiquitination [25–27]. Given this context, our finding that ACBD3 stabilizes MAVS presented a question, as ACBD3 itself lacks recognizable E3 ligases or deubiquitinase domains. To resolve this, we employed protein interaction mass spectrometry and identified the E3 ubiquitin ligase TRIM21 as a binding partner of ACBD3. Although TRIM21 is the only E3 ubiquitin ligase identified by mass spectrometry thus far, it remains unclear whether TRIM21 participates in the process by which ACBD3 stabilizes MAVS. TRIM21 has been demonstrated to stimulate the type I interferon signaling pathway during viral infection [28–30] and can restrict the replication of a wide range of viruses [31]. Furthermore, TRIM21 can promote the polyubiquitination of MAVS and facilitate the recruitment of TBK1, and the DIII domain of MAVS (aa 360-540) is the key domain for the MAVS-TRIM21 interaction [29]. Our results demonstrate that ACBD3 stabilizes MAVS levels in a TRIM21-dependent manner and that the E3 ubiquitin ligase activity of TRIM21 is partially required for maintaining MAVS stability (Supplementary Figure S8). We speculate that when ACBD3 promotes the interaction between TRIM21 and MAVS, it may occupy the active sites of other E3 ubiquitin ligases, including atrophin interacting protein 4 (AIP4) which targets K371/K420, MARCH5 which targets K500, and ring figure protein 5 (RNF5) which targets K362/K461, to their respective ubiquitination sites within the DIII domain of MAVS, inducing proteasomal degradation of MAVS, thereby stabilizing the level of MAVS [10]. This speculation still requires further experimental validation. In addition, to establish the physiological relevance of this mechanism *in vivo*, we will subsequently generate *ACBD3*-knockout mice for verification.

In summary, this study reveals a novel mechanism whereby ACBD3 exerts its antiviral function: it recruits and stabilizes TRIM21, which in turn stabilizes MAVS from degradation, leading to amplified IFN-I and ISG production and ultimately potent restriction of VSV replication. Our work thus defines the ACBD3-TRIM21-MAVS axis as a novel and crucial regulatory pathway in antiviral immunity, thereby opening new targets and avenues for therapeutic development against VSV.

Supplementary Data

Supplementary data are available at *Acta Biochimica et Biophysica Sinica* online.

Data Availability

All data generated and analyzed during this study are included in this published article and its supplementary information files. The LC-MS/MS raw data are available from the corresponding author upon reasonable request.

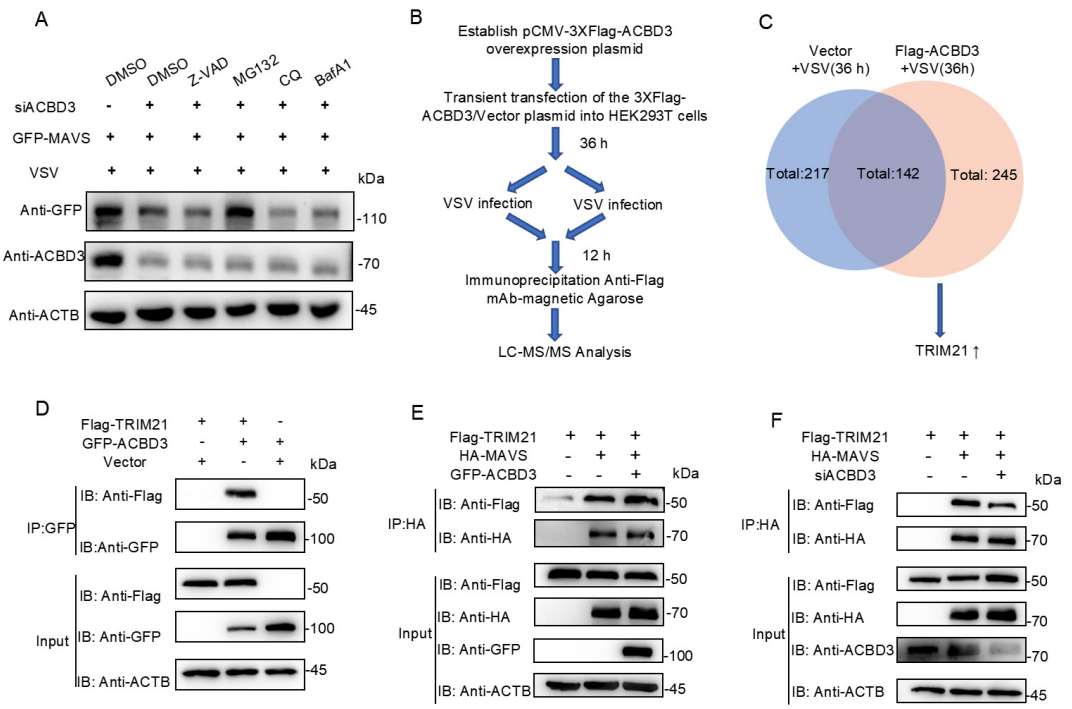


Figure 5. ACBD3 promotes the interaction between TRIM21 and MAVS (A) Western blot analysis of ACBD3 and MAVS-tagged GFP levels in HeLa cells. HeLa cells transfected with GFP-MAVS for 12 h, followed by transfection with siRNA targeting *ACBD3* for 24 h, and infected with VSV (MOI = 0.1) for 24 h. Then, cells were treated with Z-VAD, MG132, CQ, and BafA1 for 24 h. (B,C) Flow chart of protein identification that could interact with ACBD3. (D) Co-IP analysis of the interaction between ACBD3 and TRIM21. (E) ACBD3 overexpression promotes the interaction between TRIM21 and MAVS as revealed by Co-IP. (F) *ACBD3* knockdown lessens the interaction between TRIM21 and MAVS.

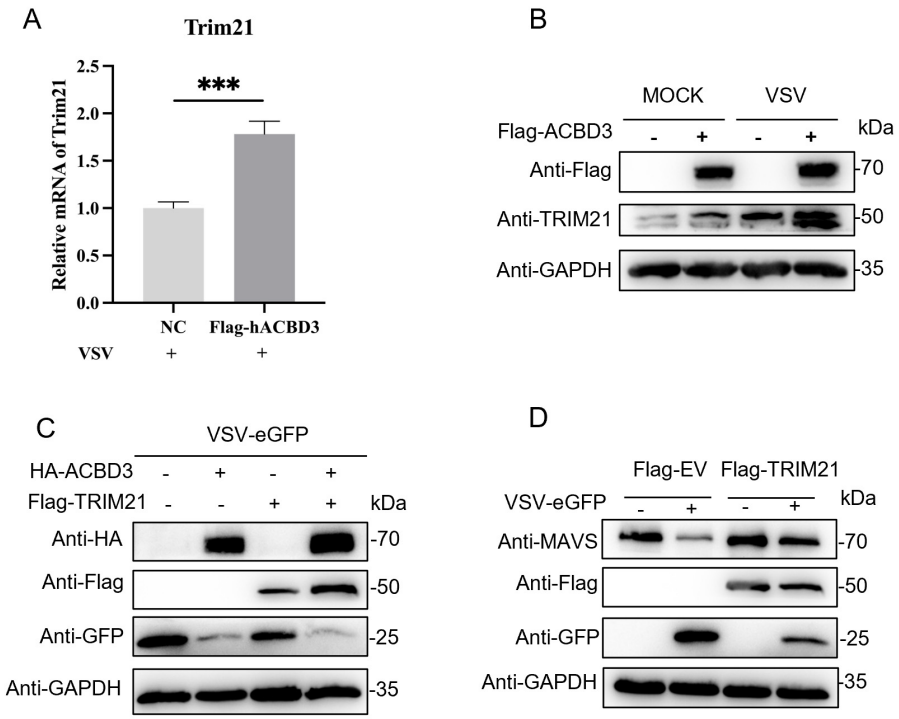


Figure 6. ACBD3 enhances the antiviral effect of TRIM21 (A) qPCR analysis of endogenous TRIM21 levels in ACBD3-overexpressing HeLa cells infected with VSV (MOI = 0.1) for 24 h. All statistical analyses were performed using GraphPad Prism 8.0. Comparisons between two groups were conducted using Student's *t* test. The mean and SD from three independent experiments are shown (***$P \leq 0.001$). (B) Western blot analysis of endogenous TRIM21 levels in ACBD3-overexpressing HeLa cells infected with VSV (MOI = 0.1) for 24 h. (C) TRIM21 overexpression suppresses MAVS degradation and viral gene expression during VSV infection, as revealed by western blot analysis. (D) TRIM21 overexpression enhances the TRIM21 protein level and suppresses viral gene expression during VSV infection.

Funding

The work was partially supported by the grants from the National Natural Science Foundation of China (No. 32373000 to P.H. and No. 32573338 to H. H.), the Taishan Scholar Young Expert Program (No. tsqn202507155 to P.H. and No. tsqnz20250714 to Y.L.), the Jinan Innovation Team (No. 202228060 to H.H.), and the Jinan Research Pioneer Workshop (No. 202333059 to H.W.).

Conflict of Interest

The authors declare that they have no conflict of interest.

References

1. Holliman A. Differential diagnosis of diseases causing oral lesions in cattle. *In Pract* 2005, 27: 2–13
2. Liu G, Cao W, Salawudeen A, Zhu W, Emeterio K, Safronetz D, Banadyga L. Vesicular stomatitis virus: from agricultural pathogen to vaccine vector. *Pathogens* 2021, 10: 1092
3. Dietzgen RG, Kondo H, Goodin MM, Kurath G, Vasilakis N. The family Rhabdoviridae: mono- and bipartite negative-sense RNA viruses with diverse genome organization and common evolutionary origins. *Virus Res* 2017, 227: 158–170
4. Jenni S, Bloyet LM, Diaz-Avalos R, Liang B, Whelan SPJ, Grigorieff N, Harrison SC. Structure of the vesicular stomatitis virus L protein in complex with its phosphoprotein cofactor. *Cell Rep* 2020, 30: 53–60.e5
5. Hastie E, Cataldi M, Marriott I, Grdzelishvili VZ. Understanding and altering cell tropism of vesicular stomatitis virus. *Virus Res* 2013, 176: 16–32
6. Iwama RE, Moran Y. Origins and diversification of animal innate immune responses against viral infections. *Nat Ecol Evol* 2023, 7: 182–193
7. Kumar H, Kawai T, Akira S. Pathogen recognition by the innate immune system. *Int Rev Immunol* 2011, 30: 16–34
8. Singh H, Koury J, Kaul M. Innate immune sensing of viruses and its consequences for the central nervous system. *Viruses* 2021, 13: 170
9. Sorouri M, Chang T, Hancks DC, Forero A, Yount J. Mitochondria and viral infection: advances and emerging battlefronts. *mBio* 2022, 13: e02096–21
10. Ren Z, Ding T, Zuo Z, Xu Z, Deng J, Wei Z. Regulation of MAVS expression and signaling function in the antiviral innate immune response. *Front Immunol* 2020, 11: 1030
11. Han W, Chen Q, Cui J, Zhao Y, Li M, Li X. E3 ubiquitin ligase RNF114 promotes vesicular stomatitis virus replication via inhibiting type I interferon production. *Microb Pathog* 2022, 167: 105569
12. Chen S, Liu Q, Zhang L, Ma J, Xue B, Li H, Deng R, *et al.* The role of REC8 in the innate immune response to viral infection. *J Virol* 2022, 96: e02175-21
13. Deng M, Tam JW, Wang L, Liang K, Li S, Zhang L, Guo H, *et al.* TRAF3IP3 negatively regulates cytosolic RNA induced anti-viral signaling by promoting TBK1 K48 ubiquitination. *Nat Commun* 2020, 11: 2193
14. Islinger M, Costello JL, Kors S, Soupene E, Levine TP, Kuypers FA, Schrader M. The diversity of ACBD proteins—from lipid binding to protein modulators and organelle tethers. *Biochim Biophys Acta* 2020, 1867: 118675
15. Chalupska D, Różycki B, Klima M, Boura E. Structural insights into Acyl-coenzyme a binding domain containing 3 (ACBD3) protein hijacking by picornaviruses. *Protein Sci* 2019, 28: 2073–2079
16. Lu Y, Song S, Zhang L. Emerging role for Acyl-CoA binding domain containing 3 at membrane contact sites during viral infection. *Front Microbiol* 2020, 11: 608
17. Chu F, Hou P, Zhu H, Gao Y, Wang X, He W, Ren J, *et al.* PBLD enhances antiviral innate immunity by promoting the p53-USP4-MAVS signaling axis. *Proc Natl Acad Sci USA* 2024, 121: e2401174121
18. Yue X, Qian Y, Gim B, Lee I. Acyl-CoA-binding domain-containing 3 (ACBD3; PAP7; GCP60): a multi-functional membrane domain organizer. *Int J Mol Sci* 2019, 20: 2028
19. Greninger AL, Knudsen GM, Betegon M, Burlingame AL, DeRisi JL. The 3A protein from multiple picornaviruses utilizes the Golgi adaptor protein ACBD3 to recruit PI4KIIIβ. *J Virol* 2012, 86: 3605–3616
20. Lei X, Xiao X, Zhang Z, Ma Y, Qi J, Wu C, Xiao Y, *et al.* The Golgi protein ACBD3 facilitates enterovirus 71 replication by interacting with 3A. *Sci Rep* 2017, 7: 44592
21. Sasaki J, Ishikawa K, Arita M, Taniguchi K. ACBD3-mediated recruitment of PI4KB to picornavirus RNA replication sites. *EMBO J* 2012, 31: 754–766
22. Mertowska P, Smolak K, Mertowski S, Grywalska E. Immunomodulatory role of interferons in viral and bacterial infections. *Int J Mol Sci* 2023, 24: 10115
23. Li D, Wu M. Pattern recognition receptors in health and diseases. *Sig Transduct Target Ther* 2021, 6: 291
24. Liu B, Gao C. Regulation of MAVS activation through post-translational modifications. *Curr Opin Immunol* 2018, 50: 75–81
25. Liu W, Yuan C, Fu B, Xie J, Li W, Zhang G, Ma Z, *et al.* E3 ubiquitin ligase ANKIB1 attenuates antiviral immune responses by promoting K48-linked polyubiquitination of MAVS. *Cell Rep* 2024, 43: 114687
26. Cheng M, Lu Y, Wang J, Wang H, Sun Y, Zhao W, Wang J, *et al.* The E3 ligase ASB3 downregulates antiviral innate immunity by targeting MAVS for ubiquitin-proteasomal degradation. *Cell Death Differ* 2024, 31: 1746–1760
27. Liu B, Zhang M, Chu H, Zhang H, Wu H, Song G, Wang P, *et al.* The ubiquitin E3 ligase TRIM31 promotes aggregation and activation of the signaling adaptor MAVS through Lys63-linked polyubiquitination. *Nat Immunol* 2017, 18: 214–224
28. Oke V, Wahren-Herlenius M. The immunobiology of Ro52 (TRIM21) in autoimmunity: a critical review. *J Autoimmunity* 2012, 39: 77–82
29. Xue B, Li H, Guo M, Wang J, Xu Y, Zou X, Deng R, *et al.* TRIM21 promotes innate immune response to RNA viral infection through Lys27-linked polyubiquitination of MAVS. *J Virol* 2018, 92: e00321-18
30. Hou P, Zhu H, Chu F, Gao Y, Sun X, Zhang F, Wang X, *et al.* Phenazine biosynthesis-like domain-containing protein (PBLD) and Cedrelone promote antiviral immune response by activating NF-κB. *Nat Commun* 2025, 16: 496
31. Bottermann M, James LC. Intracellular antiviral immunity. *Adv Virus Res* 2018, 100: 309–354